Earth Planets Space, **59**, 971–979, 2007

Simulations of superrotation using a GCM for Venus' middle atmosphere

Masaru Yamamoto[1] and Masaaki Takahashi[2]

[1]*Research Institute for Applied Mechanics, Kyushu University, 6-1 Kasuga-kouen, Kasuga, Fukuoka 816-8580, Japan*
[2]*Center for Climate System Research, University of Tokyo, 5-1-5 Kashiwanoha, Kashiwa, Chiba 277-8568, Japan*

(Received October 20, 2006; Revised April 11, 2007; Accepted April 25, 2007; Online published August 31, 2007)

A superrotation is simulated in a T10L100 general circulation model for Venus' middle atmosphere (VMAGCM), in which the radiative effects of aerosols are calculated. The simulation in a domain of 30–100 km is conducted under the condition of a bottom zonal flow with a velocity of 50 m s^{-1} at the equator. Thermal tides contribute to the maintenance of the cloud-top superrotation together with meridional circulation and vertically propagating gravity waves. The meridional circulation and wave activity are sensitive to the vertical eddy diffusion. Although the equatorial zonal flow has a velocity of about 70 m s^{-1} when the vertical eddy diffusion coefficient (K_V) is set at 5.0 m s^{-2}, it has a velocity of >100 m s^{-1} when $K_V = 2.5$ m s^{-2}. The fully developed equatorial jet for the small K_V case is enhanced at 65 km by small-scale gravity waves emitted from the cloud top.

Key words: Venus, superrotation, GCM, thermal tide.

1. Introduction

Venus' sulfuric acid clouds, which are globally observed in height regions between 48 and 70 km, play important roles in the atmospheric dynamics and sulfur cycle. Since particles and trace gases in the cloud layers are transported by the meridional circulation and waves in Venus' middle atmosphere, the dynamics can be partly inferred from brightness patterns observed in the ultraviolet (UV), infrared (IR), and near-infrared (NIR) detections. The temporal and spatial variations in the brightness provide valuable information on the atmospheric circulation and waves. Superrotational flows and planetary-scale waves with periods of 3–6 days are observed in the cloud layer (e.g., Del Genio and Rossow, 1990; Rossow *et al*., 1990), and thermal tides are observed at and above the cloud top (e.g., Schofield and Taylor, 1983). However, in comparison with Earth's atmosphere, the meteorological data are insufficient for quantitatively discussing the dynamics of Venus' atmosphere. The atmospheric dynamics have been inferred from an insufficient amount of observational data with the help of theories and numerical experiments.

General circulation model (GCM) is a useful tool for investigating the atmospheric circulation and waves in Venus' atmosphere (e.g., Yamamoto and Takahashi, 2006b); it is expected to provide a theoretical interpretation of the observational data, which will be obtained from the Venus Express and Venus Climate Orbiter. In particular, the GCM experiments are indispensable in inferring the dynamics in the regions where the meteorological data cannot be obtained by means of the explorations.

Figure 1 shows the vertical profiles of the temperatures with respect to pressure in the atmospheres of Venus and Earth (Matsuda and Matsuno, 1980). The temperature and pressure on Earth are similar to those on Venus above 50 km. This implies that Earth's GCM can be applied to Venus' middle atmosphere. In this study, a GCM for Venus' middle atmosphere (VMAGCM) is developed by suitably modifying Earth's GCM in the similar manner to that for other terrestrial planets (e.g., Leovy and Mintz, 1969); VMAGCM is utilized as the tool for investigating meridional circulation and waves in Venus' middle atmosphere. Recently, the aerosol transport models for Venus' middle atmosphere have been developed by some researchers (Imamura and Hashimoto, 1998; Yamamoto and Tanaka, 1998; Yamamoto and Takahashi, 2006a). Thus, the VMAGCM including radiative forcing of aerosols is required in order to couple with the aerosol model.

Although Venus' thermospheric general circulation models (VTGCMs) (e.g., Zhang *et al*., 1996) have already been used for the upper atmospheric sciences above 100 km, a VMAGCM has not been developed so far. Vertically propagating waves simulated in the VMAGCM are important as the momentum sources in Venus' thermosphere, and the meteorological quantities obtained from the VMAGCM are employed as the lower boundary conditions in the VTGCMs. Accordingly, the developments of both VTGCM and VMAGCM are indispensable for investigating the dynamical connection between the middle and upper atmospheres. In addition to the thermosphere, the general circulation of the middle atmosphere is connected with that of the lower atmosphere. We cannot neglect dynamical structure of meridional circulation (Schubert *et al*., 1980) and effects of thermal tides (Takagi and Matsuda, 2006) in the lower atmosphere. However, since we focus on the middle atmosphere, we do not consider the lower atmosphere in the present study.

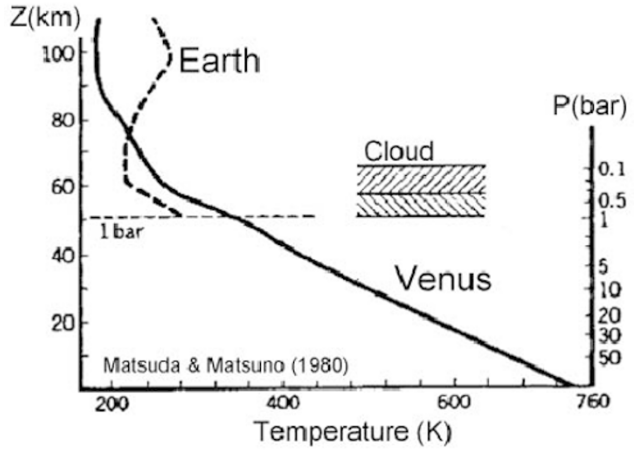

Fig. 1. Schematic diagram of the atmospheres of Venus and Earth, obtained by modifying a schematic diagram in Matsuda and Matsuno (1980).

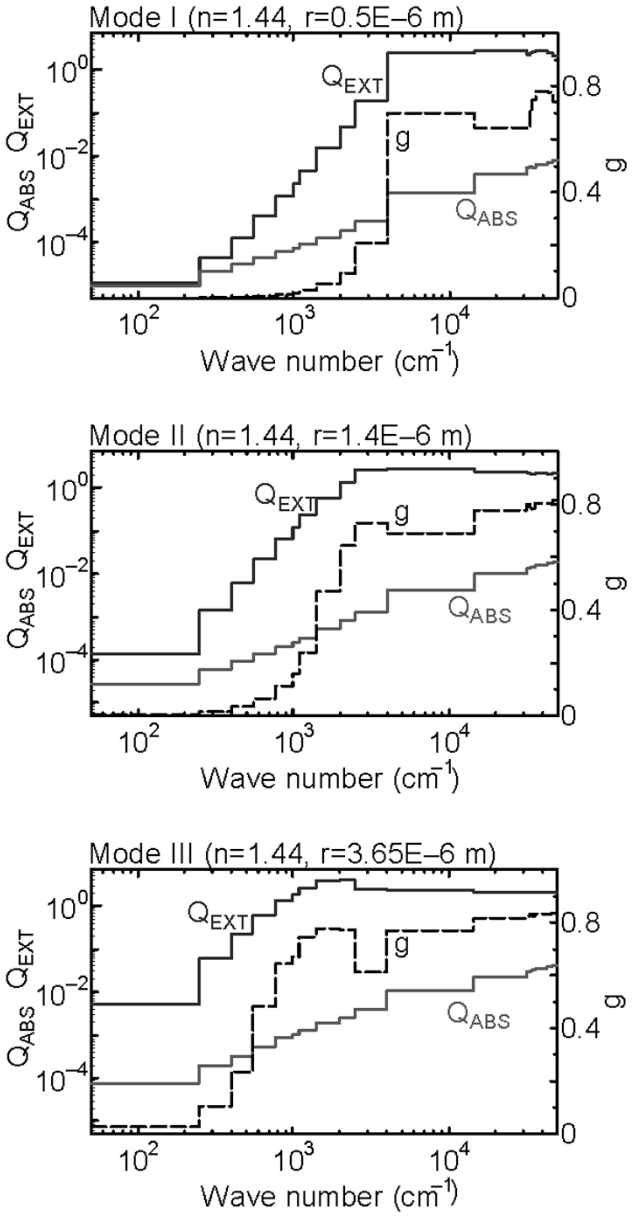

Fig. 2. Optical properties of clouds for each mode. Q_{EXT}, g, and Q_{ABS} are indicated by upper solid, dashed, and lower solid lines.

The dynamics of the middle atmosphere have been studied using spectral models with low zonal wavenumbers of 1 or 2 in previous studies (e.g., Newman and Leovy, 1992; Yamamoto and Tanaka, 1997). Newman and Leovy (1992) examined the role of thermal tides in the maintenance of the cloud-top superrotation, often termed as the "4-day circulation". Yamamoto and Tanaka (1997) examined the influences of an equatorial 4-day wave on the dynamics of the 4-day circulation, Y-shaped cloud pattern, and midlatitude 5-day wave. Instead of these simple mechanistic models, the VMAGCM including radiative forcing and nonlinear wave-wave interaction is utilized for investigating the atmospheric dynamics in the present study.

Recently, Takagi and Matsuda (2005) examined sensitivity of thermal tides in the Venus atmosphere to basic zonal flow and Newtonian cooling. However, sensitivity of the thermal tides to vertical eddy diffusion has not been sufficiently investigated in Venus AGCMs. In this paper, we focus on the influence of the vertical eddy diffusion coefficient K_V on the atmospheric dynamics. The vertically/temporally dependent K_V is parameterized by breaking of vertically propagating waves (e.g., Lindzen, 1981; Leovy, 1982). Although the vertical and temporal dependence of K_V is important in the momentum and material transport processes, K_V is assumed to be constant in our preliminary experiments, since it is difficult to incorporate realistic wave breaking into K_V on Venus. The model description is provided in Section 2; we investigate the mechanism of superrotation for large and small eddy diffusions in Section 3. Finally, the results are summarized in Section 4.

2. Model

We have developed a VMAGCM on the basis of atmospheric general circulation model developed in Center for Climate System Research/National Institute for Environmental Study (CCSR/NIES AGCM ver. 5.4) (Numaguti *et al.*, 1995), which was recently used for the atmospheres of Mars (Kuroda *et al.*, 2005) and Venus (Yamamoto and Takahashi, 2003a, 2003b, 2004, 2006b). In order to save CPU time, the truncation wavenumber is set at 10 (T10) and the vertical range from 0 to 100 km is divided into 100 layers (L100) in the sigma coordinate. The T10L100 AGCM can simulate the planetary-scale waves and atmospheric circulation. In the model, the surface topography and seasonal variations are neglected. The radiative processes in the AGCM are calculated by using a two-stream k-distribution method with 18 channels (which are divided by 50, 250, 400, 550, 770, 990, 1100, 1400, 2000, 2500, 4000, 14500, 31500, 33000, 34500, 36000, 43000, 46000, and 50000 cm^{-1}). The radiative effects of CO_2 are included in channels with wavelengths of 13.0–18.2 μm; the band and continuum absorptions of H_2O are also included. The CO_2 bands of 2.7 and 4.3-μm, which predominantly induce the radiative heating above 75 km, are not included in our model, because the dynamics below 75 km is considered in the present study. Shortwave heating in the middle atmosphere is mainly attributed to aerosols in our VMAGCM.

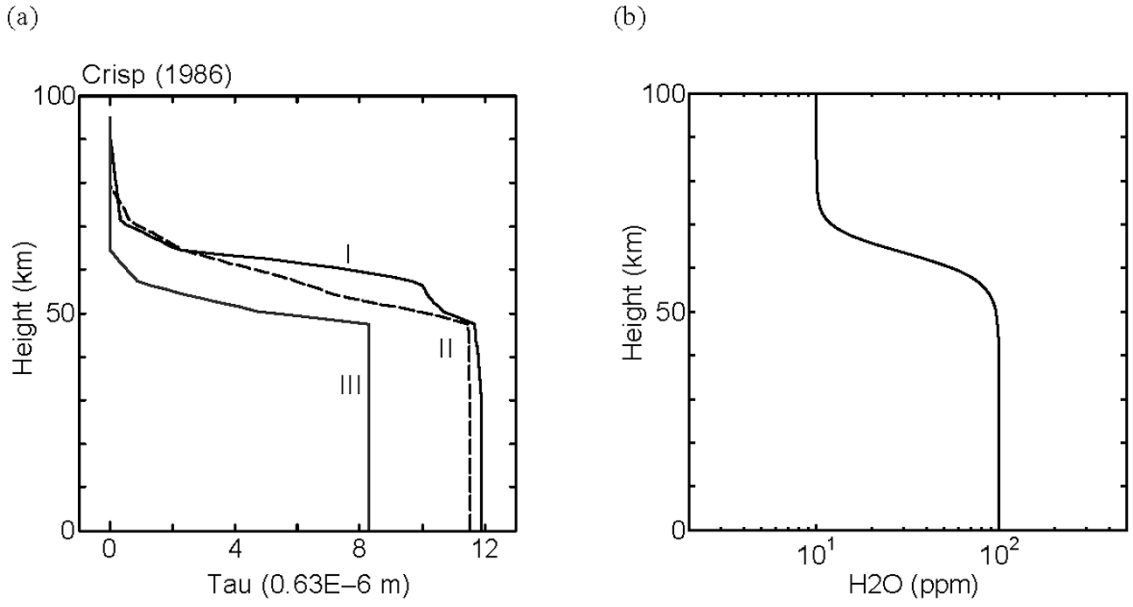

Fig. 3. Vertical distributions of (a) the cloud optical depths for each mode and (b) the H_2O mixing ratio.

The astronomical and thermodynamic parameters are modified to those of Venus', as those in Yamamoto and Takahashi (2003a, 2003b, 2004, 2006b). The planetary rotation period is set at 243 days (Earth days), a Venusian day is 117 days, the planetary radius a is 6050 km, the gravity acceleration g is 8.87 m s^{-2}, the standard surface pressure P_s is 9.2×10^4 hPa, the gas constant R is 191.4 J kg^{-1} K^{-1}, and the specific heat at constant pressure C_p is 8.2×10^2 J kg^{-1} K^{-1}.

In order to use the above-mentioned model as VMAGCM, the time integrations of temperature and wind are performed above 30 km, while they are not performed at and below 30 km. This idea originated from the numerical procedure used in the mesospheric radiative transfer model of Crisp (1986). All the diagnostic quantities, such as vertical flow, are calculated over the entire domain (0–100 km). The radiative flux emitted from below 30 km, which is employed for calculating the temperature of the middle atmosphere, is calculated by using a reference temperature below 30 km. A Rayleigh friction of 6 hours is set near the top boundary (∼100 km) in order to prevent numerical instability; further, it relaxes the horizontal flow to a motionless state (0 m s^{-1}). The coefficient α_R is defined as,

$$\alpha_R = \frac{1}{6 \text{ hours}} \left[1 + \tanh \left(\frac{z - z_T}{6 \text{ km}} \right) \right]$$

where $z = -(5 \text{ km}) \ln \sigma$ and $z_T = -(5 \text{ km}) \ln \sigma_{top}$. σ_{top} denotes the sigma level of the top layer. A fourth-order horizontal diffusion with an e-folding time of 40 days at the maximum wavenumber is applied to the model. The vertical eddy diffusion coefficient K_V is assumed to be constant. In this study, the sensitivity to K_V is discussed.

Figure 2 shows the optical properties of clouds (extinction parameter Q_{EXT}, absorption parameter Q_{ABS}, and asymmetry parameter g) calculated from the Mie scattering theory; it is assumed that sulfuric acid aerosols with a refractive index of 1.44 have radii of 0.5, 1.4, and 3.65 μm for Modes I, II, and III, respectively. The fractional scattering into the forward peak f is calculated by $f = g^2$ (Joseph *et al.*, 1976; Crisp, 1986). The vertical profiles of the optical depths for each mode at wavelength of 0.63 μm are based on the equatorial model of Crisp (1986) shown in Fig. 3(a). The optical depths at wavelength λ are given by

$$\tau_{EXT}(\lambda) = \frac{Q_{EXT}(\lambda)}{Q_{EXT}(0.63\ \mu\text{m})} \cdot \tau(0.63\ \mu\text{m}),$$

$$\tau_{SCA}(\lambda) = \frac{Q_{SCA}(\lambda)}{Q_{EXT}(0.63\ \mu\text{m})} \cdot \tau(0.63\ \mu\text{m}),$$

where subscripts *EXT* and *SCA* indicate extinction and scattering, respectively. Q_{EXT} (0.63 μm) is the extinction parameter at the channel including 0.63 μm, and τ (0.63 μm) is obtained from Fig. 3(a).

We assume 96% CO_2 in the entire region, 10 ppmv H_2O in the upper region, and 100 ppmv H_2O in the lower region (Fig. 3(b)). Although the H_2O mixing ratios are set at $\sim 10^{-3}$ at 1 bar and $\sim 10^{-5}$ at 100 bar in Crisp (1986), a constant value of 100 ppmv is assumed below 50 km in this study.

3. Results and Discussions

Several preliminary experiments were conducted in order to validate our VMAGCM and to determine the appropriate range of the physical parameters required in order to reproduce Venus' middle atmosphere. The vertical eddy diffusion coefficient K_V is one of the important quantities in dynamical and chemical models. However, it is difficult to theoretically and observationally determine the temporally/vertically dependent K_V in the middle atmosphere. In this study, we investigate the influence of constant K_V on the atmospheric dynamics. The numerical experiments are performed for $K_V = 2.5$ m^2 s^{-1} (small K_V case) and 5.0 m^2 s^{-1} (large K_V case). These values are considered to be realistic near the cloud top since a value of 4 m^2 s^{-1} near

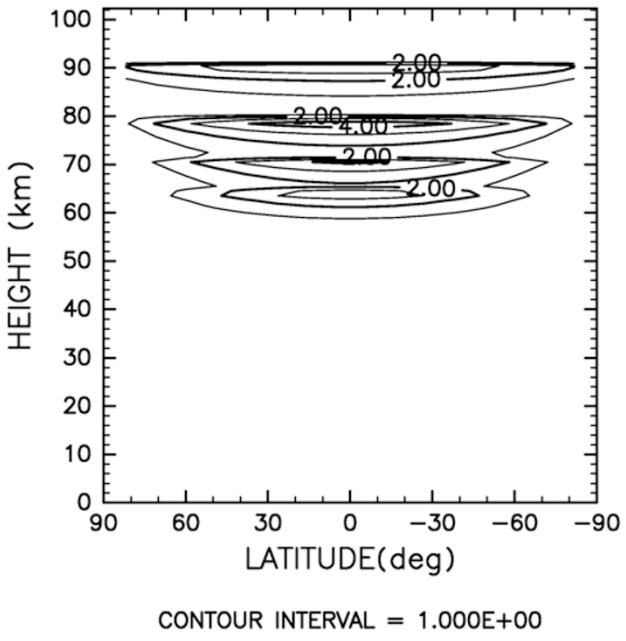

Fig. 4. Latitude-height distribution of the heating rate due to downward radiative flux for small K_V case ($K_V = 2.5$ m^2 s^{-1}).

60 km was obtained from radio scintillation measurements (Woo and Ishimaru, 1981).

The zonal flow with a rigid-body rotation of $50\cos\phi$ m s^{-1} (ϕ is the latitude) and the reference temperature (Seiff *et al*., 1980) are set as the initial conditions above 30 km, and are fixed at and below 30 km. In VMAGCM, the dynamics of the middle atmosphere are simulated under the above-mentioned conditions. The time integration is continued until the equilibrium state (4680 days) is reached.

Figure 4 shows the latitude-height distribution of the heating rate due to downward radiative flux for the small K_V case, which is the same as that for the large K_V case. As mentioned in Section 2, the simulated heating is determined from the aerosol optical depths for each mode. Heating rates of $\sim$4 K day^{-1} are seen at 64, 70, and 78 km since the aerosols with different optical depths in the three modes (Fig. 3(a)) have different heating levels for each mode. Heating at 90 km is attributed to Mode I aerosols, which marginally increases the optical thickness near 90 km.

Figures 5(a) and (b) show the latitude-height distributions of longitudinally averaged zonal flows for the small and large K_V cases, respectively. Midlatitude jets induced by the meridional circulation have velocities of >100 m s^{-1} in both the cases. The effect of K_V is insignificant in the formation of the midlatitude jets, though the jet cores are slightly shifted poleward, when K_V is increased from 5 to 10 m^2 s^{-1}. A strong equatorial superrotation with a velocity of $\sim$120 m s^{-1} is seen near 65 km for the small K_V case, however, a weak equatorial superrotation with a velocity of $\sim$70 m s^{-1} is seen near 70 km for the large K_V case. The latitude-height distribution of the mean zonal flow for the small K_V case is similar to that obtained from the Pioneer Venus radio occultation data (Newman *et al*., 1984). The equatorial jets are sensitive to K_V, differently from the midlatitude jets which are not strongly affected by K_V. This means that the magnitude of K_V is significant in the equatorial dynamics. The significance will be discussed in the later part of this section.

The residual mean meridional circulation is introduced in order to infer the circulation directly forced by the diabatic heating in the transformed Eulerian mean equation system (e.g., Andrews *et al*., 1987). Figures 6(a) and (b) show the latitude-height distributions of the residual mean meridional flows for the small and large K_V cases, respectively. The poleward flows have velocities exceeding 10 m s^{-1} near 90 km, and velocities of $\sim$3 m s^{-1} at the cloud top. Figures 7(a) and (b) show the latitude-height distributions of the residual mean vertical flows for the small and large K_V cases, respectively. The equatorial upward flow and the polar downward flow are seen in the 30–90 km region. The meridional and vertical flows in the small K_V case are stronger than those in the large K_V case. A small value of K_V leads to an increase in the meridional circulation.

Figure 8 shows the global mean angular momentum fluxes due to meridional circulation and eddies. In the same way as Yamamoto and Takahashi (2004, 2006b), the angular momentum transport due to the meridional circulation is calculated on the basis of the transformed Eulerian mean equation system, while the angular momentum transport due to the eddy momentum and heat fluxes is expressed by the Eliassen-Palm (E-P) flux (e.g., Andrews *et al*., 1987). In this study, the vertical eddy angular momentum fluxes (i.e., vertical E-P fluxes) are defined as

$$F^z_{EP} = \rho_0\, a\cos\phi\{\overline{u'w'} - [f - (\bar{u}\cos\phi)_\phi/a\cos\phi]\overline{v'\theta'}/\bar{\theta}_z\},$$

where u is the zonal flow, v is the meridional flow, w is the vertical flow, θ is the potential temperature, ρ_0 is the mean atmospheric density, a is the planetary radius, f is the Coriolis parameter, ϕ is the latitude, and z is the height. Over bar and prime represent the zonal-mean and eddy components, respectively. In this definition, a positive value represents an upward eddy angular momentum transport. The meridional circulation mostly pumps up angular momentum in the middle atmosphere, except for the lower boundary (30 km) where the vertical momentum flux due to the vertical eddy diffusion are predominant. On the other hand, as a whole, waves transport the angular momentum downward, except for 48 and 62 km. In comparison with the meridional circulation, waves do not totally contribute to pumping up of the angular momentum in the small K_V experiment. However, the upward eddy angular momentum transport cannot be neglected near 48 and 62 km in the large K_V experiment, since the transport due to the meridional circulation is small in these regions.

Figures 9(a) and (b) show the latitude-height distributions of the horizontal E-P fluxes for the small and large K_V cases, respectively. The horizontal E-P flux is defined as

$$F^\phi_{EP} = \rho_0\, a\cos\phi\,(\overline{u'v'} - \bar{u}_z\overline{v'\theta'}/\bar{\theta}_z).$$

In this definition, a positive value represents an eddy angular momentum transport from the right to the left in the panels. The horizontal eddy angular momentum flux increases near 56.5 km in the small K_V case, while the fluxes for both the cases have magnitudes of $\sim 1.5\times10^7$ kg s^{-2}

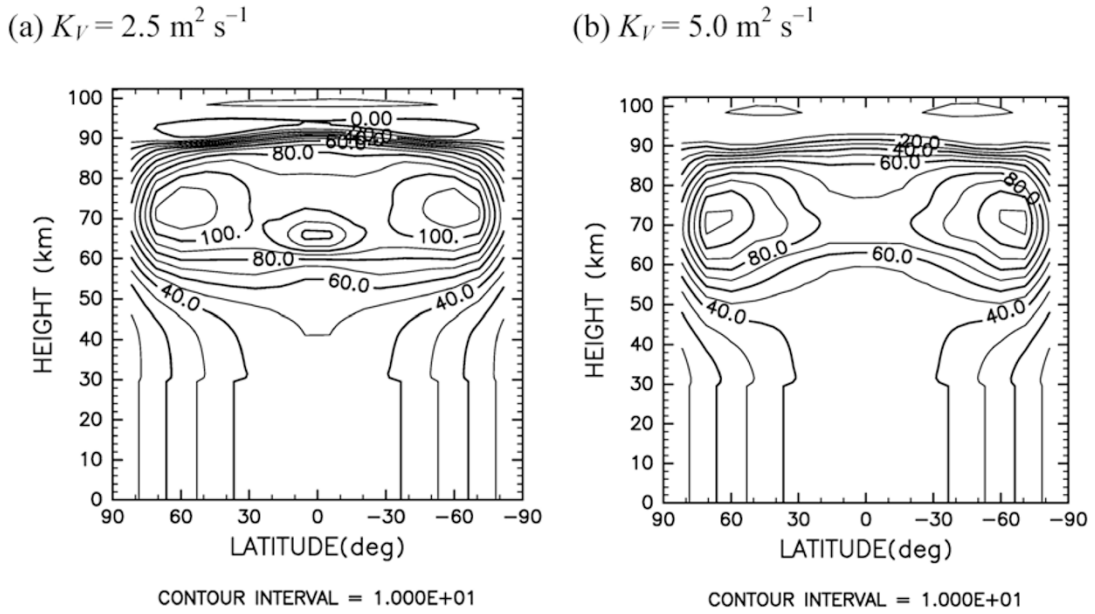

Fig. 5. Latitude-height distributions of longitudinally averaged zonal flow for (a) small K_V case ($K_V = 2.5$ m^2 s^{-1}) and (b) large K_V case ($K_V = 5.0$ m^2 s^{-1}).

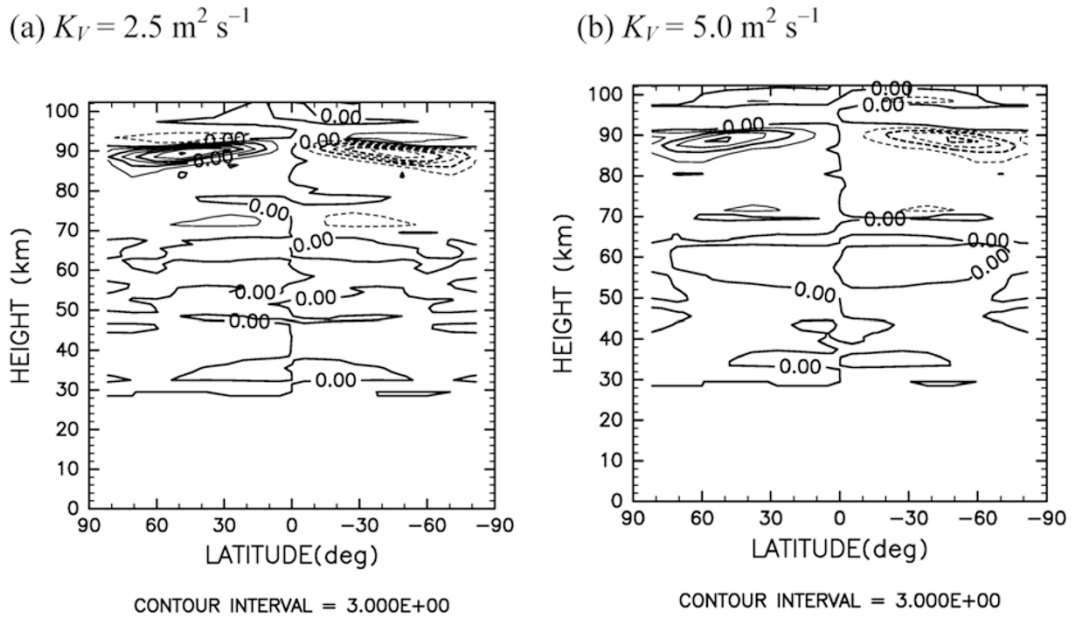

Fig. 6. Latitude-height distributions of residual mean meridional flow for (a) small K_V case ($K_V = 2.5$ m^2 s^{-1}) and (b) large K_V case ($K_V = 5.0$ m^2 s^{-1}).

at the cloud top. The latitudinal gradients of the horizontal E-P flux for the small K_V case are large at the equator when compared with large K_V. Similar to that in Yamamoto and Takahashi (2004, 2006b), thermal diurnal tides mainly transport angular momentum toward the equator in the middle atmosphere for both the cases. In addition, for the small K_V case, a midlatitude vortical wave with a period of 5.12 days and a zonal wavenumber of 1 also transports the angular momentum toward the equator near 56.5 km. The equatorward angular momentum flux of the 5.12-day wave is 2.43 times greater than that of the diurnal tide at a latitude of 27.3°. Similar to that in previous GCM experiments (e.g., Yamamoto and Takahashi, 2003a, 2006b), the global mean angular momentum flux due to the meridional circulation is upward, and the flux due to the eddy is downward. The equatorward flux near 56.5 km contributes to the equatorial acceleration; at the same time, the acceleration raises the efficiency of pumping up angular momentum since the equatorward momentum fluxes deposit enough angular momentum into the upward branch of the meridional circulation. The convergence of the equatorward momentum fluxes contributes to the maintenance of equatorial superrotation through the zonal flow acceleration. In the global view, the superrotation is mostly maintained by upward global-mean momentum flux due to the meridional circulation (Fig. 8) and equatorward eddy momentum fluxes

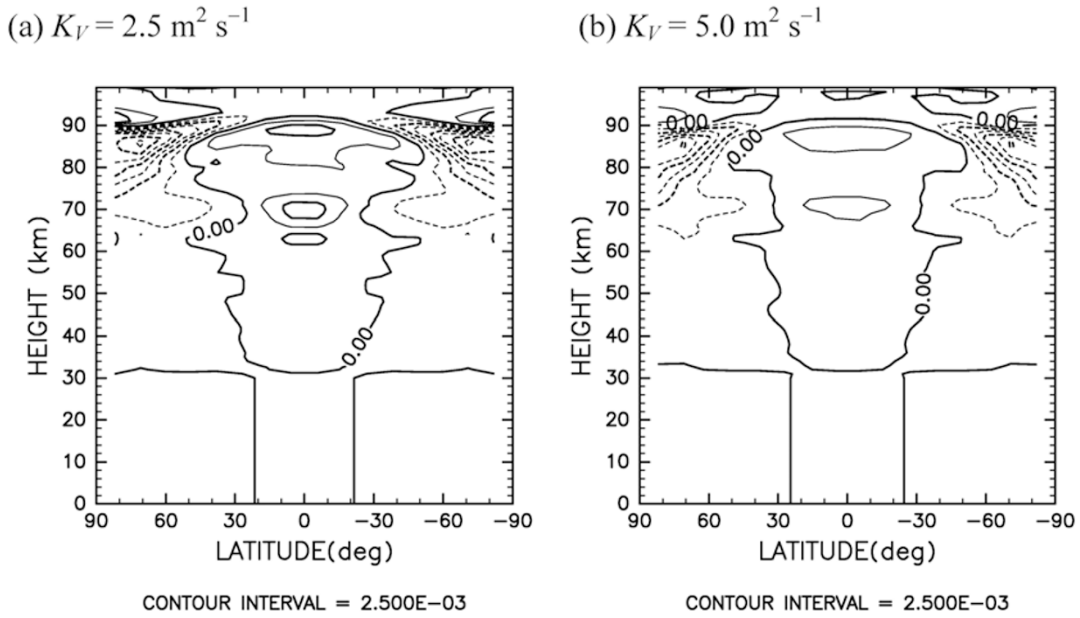

Fig. 7. Latitude-height distributions of residual mean vertical flow for (a) small K_V case ($K_V = 2.5$ m^2 s^{-1}) and (b) large K_V case ($K_V = 5.0$ m^2 s^{-1}).

(Fig. 10). Thus, the Gierasch mechanism (Gierasch, 1975; Matsuda, 1980, 1982) works in our experiments.

Figure 10 shows the vertical distributions of longitudinally averaged temperatures, residual mean vertical flows, and longitudinally averaged zonal flows at a latitude of 5.5°. For the small K_V case, the temperature is somewhat greater than that for the large K_V case; the zonal and vertical flows for the small K_V case increase in the middle atmosphere. A strong equatorial jet of ∼120 m s^{-1} is formed at 65 km. For the small K_V case, a mean upward flow of 6 mm s^{-1} (3 mm s^{-1} for the large K_V case) is seen near 70 and 90 km. Since the vertical gradient of the temperature is small near 30 km for the small K_V case (Fig. 10(a)), the temperature for the small K_V case is greater than that for the large K_V case in the region between 40 and 65 km. The temperature difference between both the cases is eliminated above 65 km since the strong vertical flow is predominant.

Figures 11(a) and (b) show the vertical profiles of the zonal flow accelerations at the equator for the small and large K_V cases, respectively. The accelerations/decelerations increase in the small K_V case. The large acceleration due to the vertical E-P flux near 65 km leads to a strong equatorial cloud-top jet. In this case, the accelerations due to the horizontal E-P flux and vertical advection are balanced with the deceleration due to the vertical E-P flux above 70 km. For the large K_V case, the acceleration due to the vertical E-P flux is small at the cloud top, and the acceleration due to the horizontal E-P flux is also small in the region between 70 and 80 km. Thus, the equatorial zonal flow for the large K_V case cannot be fully developed in the middle atmosphere.

Figures 12(a) and (b) show the spectra of vertical eddy angular momentum fluxes at a latitude of 5.5° for the small and large K_V cases, respectively. Since the sign of the vertical E-P flux of the thermal tides changes near 60 km, the thermal tides accelerate the cloud-top flow similar to that in previous studies (e.g., Newman and Leovy, 1992).

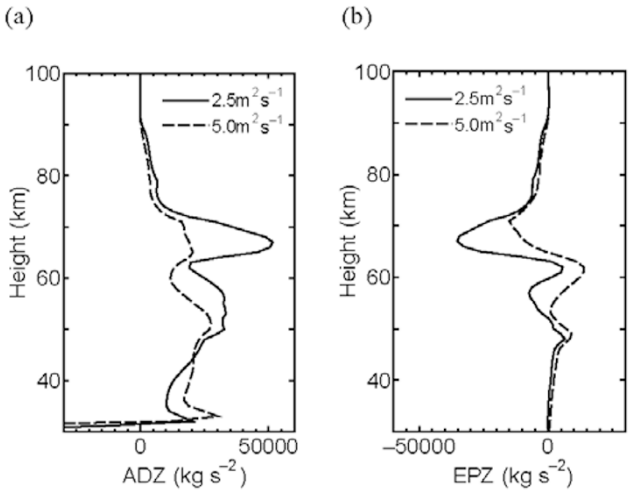

Fig. 8. Vertical profiles of global mean vertical angular momentum fluxes due to (a) meridional circulation (ADZ) and (b) eddies (EPZ) for small and large K_V cases ($K_V = 2.5$ m^2 s^{-1} and 5.0 m^2 s^{-1}, shown by solid and dashed curves, respectively).

The vertical eddy angular momentum flux of a diurnal tide is greater than that of a semidiurnal tide near the cloud top, while the flux of the semidiurnal tide is greater than that of the diurnal tide in the region of 76–90 km. This is consistent with the observations (Schofield and Taylor, 1983) in which the vertical propagation of the semidiurnal tide is apparent in the region of 70–100 km. In Fig. 12(a), for the small K_V case, in addition to the E-P flux of the thermal tides, we can see large vertical E-P fluxes caused by small-scale equatorial gravity waves with phase velocities of ∼100 m s^{-1} and a wavenumber of 10 near the cloud top. They are similar to those in Yamamoto and Takahashi (2003a). The small-scale equatorial gravity waves largely accelerate the fully developed equatorial jet at 65 km, and decelerated it near 70 km. Although the E-P flux of each

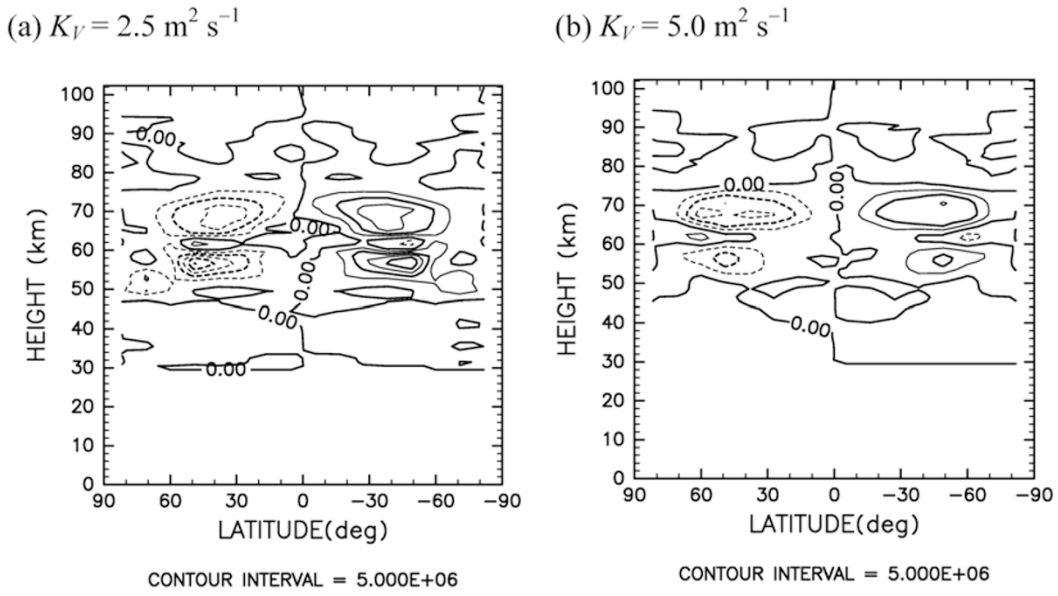

Fig. 9. Latitude-height distributions of horizontal E-P flux for (a) small K_V case ($K_V = 2.5$ m^2 s^{-1}) and (b) large K_V case ($K_V = 5.0$ m^2 s^{-1}).

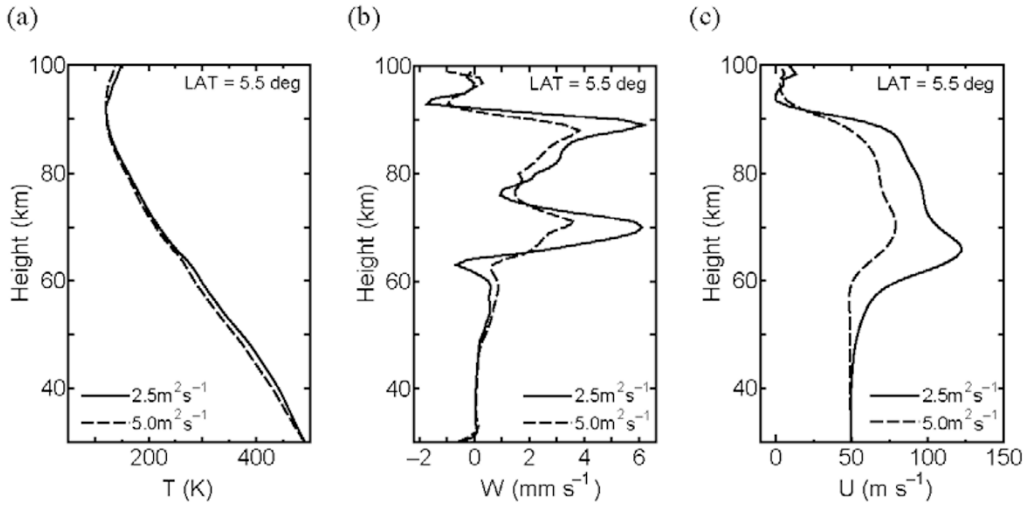

Fig. 10. Vertical profiles of (a) zonal mean temperature, (b) residual mean vertical flow, and (c) zonal mean flow at a latitude of 5.5° for small and large K_V cases ($K_V = 2.5$ m^2 s^{-1} and 5.0 m^2 s^{-1}, shown by solid and dashed curves, respectively).

small-scale gravity wave is too small to see below 60 km in Fig. 12(a), the total flux of the many waves is downward and greater than the upward flux of the thermal tides in the equatorial region between 40 and 60 km. Thus the total vertical E-P flux of all the waves is downward at the equator above 40 km for the large K_V case (not shown).

The vertical propagation of the thermal tides is sensitive to the vertical distributions of the zonal mean winds through the intrinsic phase velocity $c - \bar{u}$ above 60 km. Due to small K_V, increases of the meridional circulation and fast small-scale waves lead to a change in the zonal mean flow through the zonal flow acceleration; this alters the vertical angular momentum fluxes of the thermal tides. Below 60 km where the radiative damping of the thermal tides is ineffective, the thermal tides are sensitive to K_V. The vertical angular momentum flux for the small K_V case is greater than that for the large K_V case in the equatorial region.

Finally, the thermal tides in the small K_V case (in which strong superrotation is reproduced) are compared with those in the observation. With regard to the temperature component of the diurnal tide, in the small K_V case, the peaks of 3.8 K at a latitude of 70° (1.5 K at a latitude of 60° for the Pioneer Venus orbiter infrared radiometer (OIR) channel 3, Elson, 1983; Pechmann and Ingersoll, 1984) and 1.6 K at the equator (1.5 K for the OIR channel 3) are seen at 70.5 km; further the midlatitude phase is by 120° ahead of the equatorial one. The diurnal-tide peak of 3.2 K at a latitude of 70° (2.0 K and 4.5 K at a latitude of 65° for the OIR channels 4 and 5, respectively) is seen at 65.5 km in this case; however, the polar OIR temperature peak observed at a latitude of 80° is not reproduced in this model.

In the small K_V case, the semidiurnal tide has a temperature component of 1 K within latitudes of ±60° at 70.5 km, which is lower than that of the OIR channel 3 (3.5 K). The semidiurnal midlatitude peak of 0.7 K is seen at a latitude of 50° at 65.5 km. This is smaller than those of the

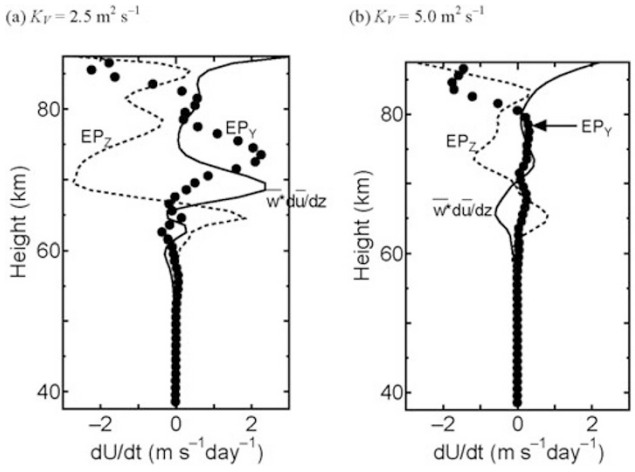

Fig. 11. Vertical profiles of zonal flow accelerations at the equator for (a) small K_V case (K_V = 2.5 m^2 s^{-1}) and (b) large K_V case (K_V = 5.0 m^2 s^{-1}) at the equator. The solid curve indicates the vertical advection, the dashed curve indicates the vertical E-P flux convergence, and the circle indicates the horizontal E-P flux convergence.

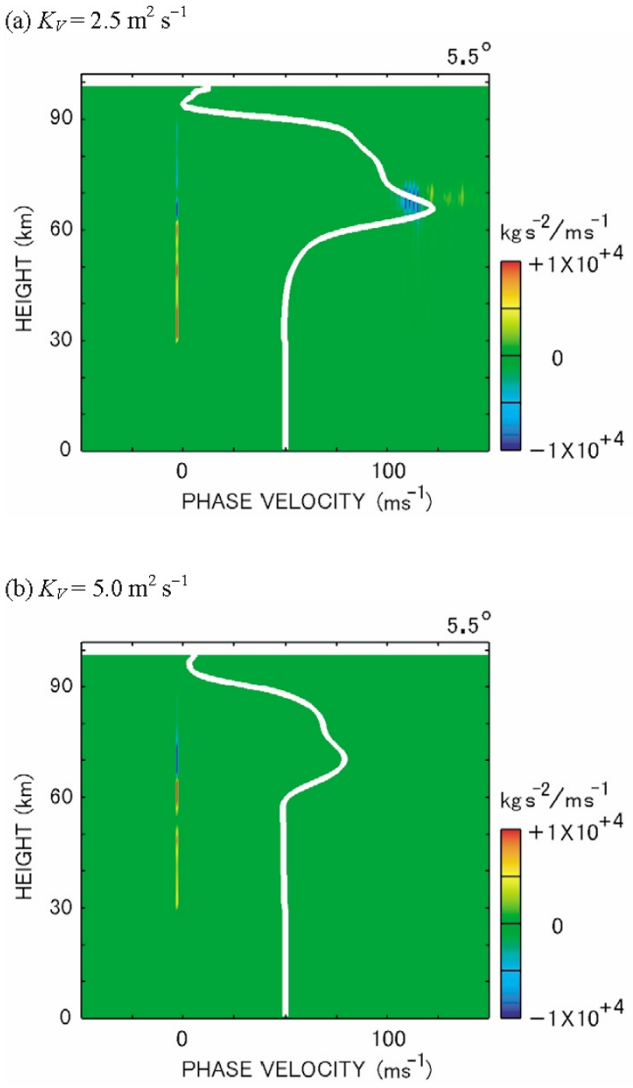

Fig. 12. Phase velocity-latitude distributions of vertical E-P flux for (a) small K_V case (K_V = 2.5 m^2 s^{-1}) and (b) large K_V case (K_V = 5.0 m^2 s^{-1}) at a latitude of 5.5°.

OIR channels 4 and 5 (1.5 K and 2.5 K at a latitude of 70°, respectively).

4. Concluding Remarks

We applied the T10L100 CCSR/NIES AGCM to a GCM for Venus' middle atmosphere (VMAGCM), in which the radiative effects of aerosols are calculated, and simulated the atmospheric circulation and waves in the superrotation. In the present study, we focus on the influence of vertical eddy diffusion on the atmospheric dynamics. The midlatitude jets are insensitive to K_V, while the equatorial jets are strongly affected by K_V. This means that the vertical eddy diffusion influences the equatorial superrotation and its maintenance mechanism. The superrotation is fully developed near the cloud top for the small K_V (=2.5 m^2 s^{-1}) experiment. The meridional circulation for the small K_V case is stronger than that for the large K_V (=5.0 m^2 s^{-1}) case. Large zonal flow accelerations due to waves and advection are seen at the equator in the small K_V case. The horizontal E-P flux above 70 km, vertical advection near 70 km, and vertical E-P flux near 65 km accelerate the equatorial superrotation. In both the small and large K_V cases, thermal tides contribute to the maintenance of superrotation (e.g., Fels and Lindzen, 1974; Newman and Leovy, 1992), together with meridional circulation. When small K_V is set in the model, in addition to thermal tides, a 5.12-day vortical wave also generates equatorward angular momentum flux near 56.5 km, and small-scale equatorial gravity waves with velocities of ∼100 m s^{-1} also generate vertical angular momentum flux. In particular, the small-scale equatorial gravity waves enhance the equatorial jet at the cloud top through the large acceleration due to the vertical E-P flux.

As mentioned above, the meridional circulation and small-scale wave activity increase in the small K_V case. The increases in the meridional circulation and small-scale wave activity lead to large accelerations of the equatorial zonal flow due to advection and E-P fluxes. These large accelerations caused by the small K_V enhance the equatorial superrotation.

Based on the global mean angular momentum transport, the simulated superrotations are maintained by the meridional circulation. Accordingly, the global maintenance mechanism of the superrotation is identified as the Gierasch one (e.g., Gierasch, 1975; Matsuda, 1980, 1982). For the large K_V case, waves partly contribute to pumping-up of angular momentum. This is different from our previous experiments (Yamamoto and Takahashi, 2006b). On the other hands, the regional maintenance of the equatorial cloud-top superrotation is caused by vertical and horizontal E-P fluxes of thermal tides and gravity waves (e.g., Fels and Lindzen, 1974; Newman and Leovy, 1992). The equatorial acceleration due to these waves enhances the efficiency of upward angular momentum transport in the Gierasch mechanism. The global maintenance mechanism of the superrotation is mostly explained by the theory of Gierasch, while the equatorial maintenance mechanism is explained by the theories of Fels and Lindzen (the equatorial acceleration by the vertical EP flux) and Gierasch (the equatorial accelera-

tion by the horizontal EP flux). This is consistent with Yamamoto and Takahashi (2006b), though they emphasized the Gierasch mechanism in their paper. The two theories of Fels and Lindzen (1974) and Gierasch (1975) coexist in the maintenance mechanism of the superrotation.

As the next step, we envisage to improve the radiative properties of CO_2 and aerosols and apply the VMAGCM to the dynamics of superrotation and brightness patterns observed in the middle atmosphere.

Acknowledgments. We would like to thank Dr. M. D. Yamanaka and an anonymous reviewer for helpful comments and suggestions. This study is supported by the Cooperative Research Project of the Center for Climate System Research, University of Tokyo, and by the JSPS Grant-in-Aid for Young Scientists (B) (No. 17740313). In this study, the results are partly obtained using the supercomputing resources at the Information Synergy Center, Tohoku University. The GFD-DENNOU library is used in drawing the figures.

References

Andrews, D. G., J. R. Holton, and C. B. Leovy, *Middle Atmosphere Dynamics*, 489 pp., Academic Press, San Diego, 1987.

Crisp, D., Radiative forcing of the Venus mesosphere I. Solar fluxes and heating rates, *Icarus*, **67**, 484–514, 1986.

Del Genio, A. D. and W. B. Rossow, Planetary-scale wave and the cyclic nature of cloud top dynamics on Venus, *J. Atmos. Sci.*, **47**, 293–318, 1990.

Elson, L. S., Solar related waves in the Venusian atmosphere from the cloud tops to 100 km, *J. Atmos. Sci.*, **40**, 1535–1551, 1983.

Fels, S. B. and R. S. Lindzen, The interaction of thermally excited gravity waves with mean flows, *Geophys. Fluid Dynamics*, **6**, 149–191, 1974.

Gierasch, P. J., Meridional circulation and the maintenance of the Venus atmosphere rotation, *J. Atmos. Sci.*, **32**, 1038–1044, 1975.

Imamura, T. and G. L. Hashimoto, Venus cloud formation in the meridional circulation, *J. Geophys. Res.*, **103**, 31349–31366, 1998.

Joseph, J. H., W. J. Wiscombe, and J. H. Weinman, The Delta-Eddington approximation for radiative flux transfer, *J. Atmos. Sci.*, **33**, 2452–2459, 1976.

Kuroda, T., N. Hashimoto, D. Sakai, and M. Takahashi, Simulation of the Martian atmosphere using a CCSR/NIES AGCM, *J. Meteor. Soc. Japan*, **83**, 1–15, 2005.

Leovy, C., Control of the homopause level, *Icarus*, **50**, 311–321, 1982.

Leovy, C. and Y. Mintz, Numerical simulation of the atmospheric circulation and climate of Mars, *J. Atmos. Sci.*, **26**, 1167–1190, 1969.

Lindzen, R. S., Turbulence and stress due to gravity waves and tidal breakdown, *J. Geophys. Res.*, **86**, 9707–9714, 1981.

Matsuda, Y., Dynamics of the four-day circulation in the Venus atmosphere, *J. Meteor. Soc. Japan*, **58**, 443–470, 1980.

Matsuda, Y., A further study of dynamics of the four-day circulation in the Venus atmosphere, *J. Meteor. Soc. Japan*, **60**, 245–254, 1982.

Matsuda, Y. and T. Matsuno, 4-day circulation in the Venus atmosphere, *Kagaku*, **50**, 285–293, 1980 (in Japanese).

Newman, M. and C. B. Leovy, Maintenance of strong rotational winds in Venus' middle atmosphere by thermal tides, *Science*, **257**, 647–650, 1992.

Newman, M., G. Schubert, A. J. Kliore, and I. R. Patel, Zonal winds in the middle atmosphere of Venus from Pioneer Venus radio occultation data, *J. Atmos. Sci.*, **41**, 1901–1913, 1984.

Numaguti, A., M. Takahashi, T. Nakajima, and A. Sumi, Development of an atmospheric general circulation model, in *Climate System Dynamics and Modelling*, vol. I-3, edited by T. Matsuno, pp. 1–27, Cent. for Clim. Syst. Res., Univ. of Tokyo, Tokyo, 1995.

Pechmann, J. B. and A. P. Ingersoll, Thermal tides in the atmosphere of Venus: Comparison of model results with observations, *J. Atmos. Sci.*, **41**, 3290–3313, 1984.

Rossow, W. B., A. D. Del Genio, and T. Eichler, Cloud-tracked winds from Pioneer Venus OCPP images, *J. Atmos. Sci.*, **47**, 2053–2084, 1990.

Schofield, J. T. and F. W. Taylor, Measurements of the mean, solar-fixed temperature and cloud structure of the middle atmosphere of Venus, *Quart. J. R. Met. Soc.*, **109**, 57–80, 1983.

Schubert, G., C. Covey, A. D. Del Genio, L. S. Elson, G. Keating, A. Seiff, R. E. Young, J. Apt, C. C. Counselman, III, A. J. Kliore, S. S. Limaye, H. E. Revercomb, L. A. Sromovsky, V. E. Suomi, F. Taylor, R. Woo, and U. von Zahn, Structure and circulation of the Venus atmosphere, *J. Geophys. Res.*, **85**, 8007–8025, 1980.

Seiff, A., D. B. Kirk, R. E. Young, R. C. Blanchard, J. T. Findlay, G. M. Kelly, and S. C. Sommer, Measurements of thermal structure and thermal contrasts in the atmosphere of Venus and related dynamical observations: Results from the four Pioneer Venus probes, *J. Geophys. Res.*, **85**, 7903–7933, 1980.

Takagi, M. and Y. Matsuda, Sensitivity of thermal tides in the Venus atmosphere to basic zonal flow and Newtonian cooling, *Geophys. Res. Lett.*, **32**, L02203, doi:10.1029/2004GL022060, 2005.

Takagi, M. and Y. Matsuda, Dynamical effect of thermal tides in the lower Venus atmosphere, *Geophys. Res. Lett.*, **33**, L13102, doi:10.1029/2006GL026168, 2006.

Woo, R. and A. Ishimaru, Eddy diffusion coefficient for the atmosphere of Venus from radio scintillation measurements, *Nature*, **289**, 383–384, 1981.

Yamamoto, M. and H. Tanaka, Formation and maintenance of the 4-day circulation in the Venus middle atmosphere, *J. Atoms. Sci.*, **54**, 1472–1489, 1997.

Yamamoto, M. and H. Tanaka, The Venusian Y-shaped cloud pattern based on an aerosol-transport model, *J. Atmos. Sci.*, **55**, 1400–1416, 1998.

Yamamoto, M. and M. Takahashi, The fully developed superrotation simulated by a general circulation model of a Venus-like atmosphere, *J. Atmos. Sci.*, **60**, 561–574, 2003a.

Yamamoto, M. and M. Takahashi, Superrotation and equatorial waves in a T21 Venus-like AGCM, *Geophys. Res. Lett.*, **30**, doi:10.1029/2003GL016924, 2003b.

Yamamoto, M. and M. Takahashi, Dynamics of Venus' superrotation: the eddy momentum transport processes newly found in a GCM, *Geophys. Res. Lett.*, **31**, doi:10.1029/2004GL019518, 2004.

Yamamoto, M. and M. Takahashi, An aerosol transport model based on a two-moment microphysical parameterization in the Venus middle atmosphere: model description and preliminary experiments, *J. Geophys. Res.*, **111**, doi:10.1029/2006JE002688, 2006a.

Yamamoto, M. and M. Takahashi, Superrotation maintained by meridional circulation and waves in a Venus-like AGCM, *J. Atmos. Sci.*, **63**, 3296–3314, 2006b.

Zhang, S., S. W. Bougher, and M. J. Alexander, The impact of gravity waves on the Venus thermosphere and O_2 IR nightglow, *J. Geophys. Res.*, **101**, 23195–23205, 1996.

M. Yamamoto (e-mail: yamakatu@riam.kyushu-u.ac.jp) and M. Takahashi (e-mail: masaaki@ccsr.u-tokyo.ac.jp)